Temporal contrast of a post-compressed Yb:YAG burst-mode laser

Anne-Lise Viotti,[1,2] Skirmantas Alisauskas,[1] Henrik Tünnermann,[1] Esmerando Escoto,[1] Marcus Seidel,[1] Katharina Dudde,[1] B. Manschwetus,[1] Ingmar Hartl,[1] Christoph M. Heyl[1,3,4]

[1]*Deutsches Elektronen-Synchrotron DESY, Notkestraße 85, 22607 Hamburg, Germany.*
[2]*Department of Physics, Lund University, P.O Box 118, SE-221 00 Lund, Sweden.*
[3]*Helmholtz-Institute Jena, Fröbelstieg 3, 07743 Jena, Germany.*
[4]*GSI Helmholtzzentrum für Schwerionenforschung GmbH, Planckstraße 1, 64291 Darmstadt, Germany.*
**Corresponding author: anne-lise.viotti@desy.de*

Received XX Month XXXX; revised XX Month, XXXX; accepted XX Month XXXX; posted XX Month XXXX (Doc. ID XXXXX); published XX Month XXXX

Combining the high average power of Ytterbium (Yb)-based lasers with post-compression techniques constitutes a very attractive approach to reach shorter pulse durations and higher peak powers. While an excellent spatial pulse quality is commonly reached, the peak power is typically limited by temporal contrast characteristics which are intrinsic to the post-compression process. Employing spectral broadening of a burst-mode Yb:YAG laser in a gas-filled multi-pass cell, we reach a relative energy content close to the theoretical limit of up to 78% compared to the full pulse energy including the ps background at a compression factor of 13, yielding pulses with 56 fs duration. Our results are based on a reliable intra-burst characterization of temporal contrast, spectrum, phase and pulse duration at 100 kHz repetition rate, demonstrating attractive pulse parameters e.g. for pump-probe spectroscopy. They further promise applicability of post-compressed lasers employing large compression factors as efficient drivers for secondary frequency conversion stages.

Ultrafast high-average-power, mJ-class lasers have become essential tools for many scientific and industrial applications within multiple fields including AMO physics, chemistry, material science, or material processing [1]. While Titanium Sapphire-based systems can easily reach pulse durations below 30 femtoseconds (fs), they are limited in average power. In contrast, Ytterbium (Yb) systems are power-scalable into the kW regime [2,3] as they can easily be diode-pumped but their pulse duration is gain bandwidth-limited to a few 100 fs up to about 1 ps. Many applications, e.g., attosecond science, laser-based particle acceleration, or X-ray Free Electron Laser (FEL) science employing optical pump-probe lasers would greatly benefit from combining the high average power characteristics of Yb lasers with shorter pulse durations. Nonlinear pulse post-compression methods utilizing spectral broadening followed by chirp removal provide a viable approach to reach this goal. Different techniques have been employed to date including multi-plate continuum generation, multi-pass cells (MPCs), photonic-crystal fiber, and hollow-core fiber-based spectral broadening or self-compression (see [4] and references therein for a complete overview). Despite the large parameter and application range covered by post-compression methods, there is a key challenge that has not attracted much attention until today: the intrinsically limited temporal pulse contrast of post-compressed pulses. High order phase contributions from self-phase modulation (SPM) remaining after compression and typical spectral amplitude modulations cause the appearance of pre- and post-pulses or long pedestals, limiting the energy content of the main compressed pulse especially at large compression ratios and thus restricting the effective peak power boost. In particular, non-optimal compression can affect the temporal contrast. In this context, burst-mode lasers with non-continuous repetition rate employed e.g. as FEL pump-probe lasers, present additional challenges as the post-compression process couples input pulse energy instabilities with output pulse parameters. Precise characterization and control of intra-burst pulse dynamics is therefore crucial.

The temporal contrast of ultrashort pulses is often quantified as intensity contrast. In high-field physics, such as laser-driven particle acceleration, a high intensity contrast is typically required at long delays (ps to ns regime). Contrast improvement techniques employing e.g. cross-phase modulation or nonlinear elliptical polarization rotation [5,6] have been employed but reduce the energy in the main peak [7]. Contrarily, for applications such as ultrafast pump-probe spectroscopy at moderate laser intensities, the temporal pulse energy contrast and/or peak power is of main

interest while relaxed intensity contrast requirements exist. Consequently, our efforts address mainly the temporal energy contrast. Reports on pulse post-compression often focus on the full width at half maximum (FWHM) of the pulse duration of the compressed pulse, typically characterized by low-dynamic range autocorrelators (ACs) or second harmonic frequency resolved optical gating (SHG-FROG), while neglecting energy content in the temporal pulse pedestal. This brings along the risk to overestimate pulse energy contrast and peak power. Gröbmeyer et al. reported 45% energy content in the compressed pulse out of a bulk multi-pass setup with a compression factor of 9.6 [8], while Köttig et al. reported an energy content fraction between 63% and 67% (compression factor of 13.6) after a photonic crystal fiber setup [9]. Up to 80% in the main post-compressed peak was reported with a kW gas-filled multi-pass cell (MPC) for a smaller compression factor of 6 [10].

In this Letter, we investigate the energy content of post-compressed pulses at large compression ratios (>10) employing an Yb:YAG burst-mode laser with high intra-burst repetition rate (100 kHz) and high average power (320 W), post-compressed in a gas-filled MPC. We characterize individual pulses inside the burst at 100 kHz repetition rate. Third-order autocorrelation measurements reveal a relative energy content of up to 78 % in the main post-compressed pulse and a stable broadened spectrum and compressed pulse duration within the flat part of the burst. To the best of our knowledge, this is the first demonstration of such a high relative energy content of a post-compressed pulse at high (>10) compression ratio including a reliable characterization of pre-/post- pulses and picosecond (ps) pedestal.

At the FEL facility FLASH in Hamburg [11], burst mode lasers matching the temporal structure of the FEL pulse [12] are employed. Recent laser concepts for the planned FLASH upgrade [13] employ high average power Yb:YAG lasers together with MPCs for spectral broadening and subsequent pulse compression [14,15], provide simplified solutions compared to traditional optical parametric chirped pulse amplification (OPCPA) approaches. MPCs offer high throughput, large compression ratios [16], good beam quality [17], and great possibilities for average power [10] and pulse energy scaling [18]. In this Letter, we use the FLASH2 burst-mode pump-probe laser [12] with a gas -filled MPC post-compression setup. It consists of an Yb laser frontend which seeds a Yb:YAG Innoslab chirped pulse amplifier (CPA) [18]. Conventionally, the CPA is used as the pump source for an OPCPA system. In our experiment, the output of the amplifier is directly post-compressed [15,16], as depicted in Fig. 1. The system delivers up to 320 W in 10 Hz burst (3.2 mJ single pulse energy at 100 kHz repetition rate) at 1030 nm, with a current pulse duration of 730 fs FWHM.

The pulses are spectrally broadened in an MPC filled with 1 bar of Argon. The cell is used in a near-concentric configuration and consists of two dielectric broadband concave mirrors with radius of curvature of 1 m and a diameter of 100 mm. The MPC is operated with 18 roundtrips and about 87% transmission efficiency. A lens telescope is used to mode-match the laser beam to the MPC eigenmode. A broadened spectrum is shown in Fig. 1. The output of the cell is then compressed using transmission gratings insensitive to polarization in a compact 4 pass compressor configuration. Out-coupling of the compressor is performed via a broadband thin film polarizer operating at 70° . After the compressor, the post-compressed pulses are sent to a fully automated home-built non-collinear 3rd order AC. The AC is able to resolve up to 4.5 orders of magnitude of pulse intensity contrast, limited by the dynamic range of the current electronic detection system consisting of a sensitive ultraviolet (UV) photodiode together with neutral density filters, see Fig. 2 (a)-(c).

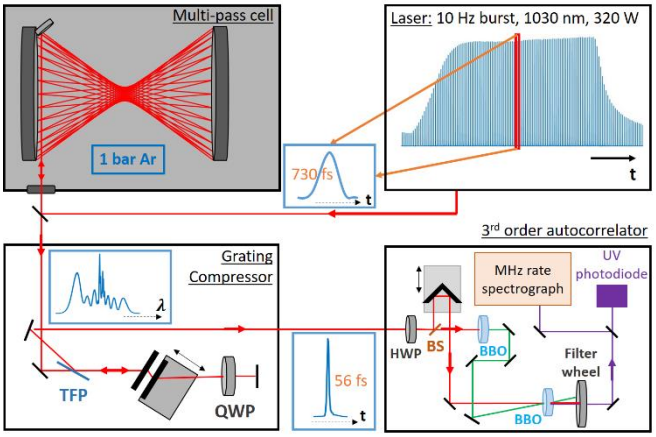

Fig. 1. Schematic of the experimental setup. TFP: thin film polarizer, BS: beam splitter, QWP/HWP: quarter/half wave plate. The input pulse profile from the Innoslab CPA amplifier, the spectrally broadened output of the MPC and the pulse after the compressor are shown in the blue inset panels.

For our experiment, the MPC was operated at a spectral broadening setting leading to compressed pulse durations of about 56 fs FWHM, estimated via AC measurements. Fig. 2 (a) shows a single pulse intensity AC trace recorded employing the full dynamic range of our device (blue) enabled by the combination of neutral density filters together with the linear response regime of the photodiode. It is compared in logarithmic scale with a similar measurement performed using a single neutral density filter as used in most FROG or autocorrelator devices (orange), illustrating the need for a reliable contrast measurement at high dynamic range. The corresponding post-compressed pulse AC trace is shown in linear scale in Fig. 2 (b). The shaded area in (b) depicts the integration window used for deriving the energy content in the compressed peak. We chose twice the FWHM of the post-compressed pulse duration τ and compare the energy content in this window with the energy contained in the full 5 ps scanning window. We obtain a relative energy content of 78% in the main compressed pulse, measured via 3rd order AC for a compression ratio of 13 at 320 W in-burst input average power. While the reported result corresponds to a slightly chirped pulse (Fourier limit: 52 fs), we achieve a high temporal energy contrast very close to the theoretical limit (red data point in (d)). Theoretical predictions based on nonlinear pulse propagation simulations [19] considering large compression ratios are also shown in (d). The solid line represents the calculated relative energy content in the main compressed peak for a Fourier transform-limited (FTL) pulse, using the integration window defined above, assuming a perfect Gaussian input pulse. The influence of the remaining chirp onto the experimentally measured energy contrast could be quantified by reconstructing the corresponding FTL pulse from third-order FROG measurements (see details below). The reconstructed energy content is depicted via a data point in (d). Detailed studies on the impact of dispersion and compression ratio onto the compression quality will be reported in a separate publication [20].

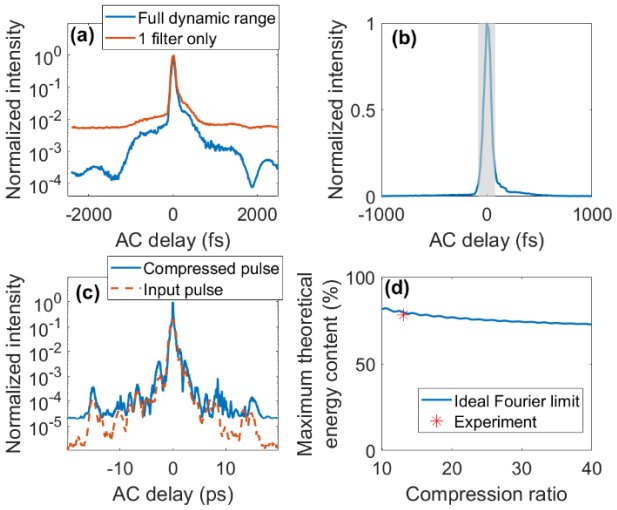

Fig. 2. (a) AC traces revealing the temporal contrast of a single post-compressed pulse in the burst shown in log scale at full dynamic range of the 3rd order autocorrelator (blue) and for a single filter (orange). (b) AC results corresponding to (a) in linear scale at full dynamic range. The integration window (2τ) used for the energy content estimation is shown (shaded area). (c) AC trace for a 40 ps scanning window, comparing the post-compressed pulse with the uncompressed laser output (dotted line). (d) Simulated theoretical limit for the maximum energy content achievable with a transform-limited post-compressed pulse (solid line together with the experimental data point (red star).

Fig. 2 (c) depicts the AC trace over the full scanning window of the AC setup, i.e. 40 ps, and shows that the pre- and post-pulses have an intensity of less 0.5% compared to the main peak at time delays larger than 2.5 ps. Peaks at longer time delays are also present in the initial pulse from the Yb amplifier (see dotted orange curve) and, as such, are not inherent to post-compression. The AC traces are recorded with 50 fs steps for the 40 ps scanning window and 10 fs steps for the 5 ps window.

Using the relative energy content of the main compressed pulse, we can easily estimate the real peak power enhancement reached with the given post-compression method. For instance, for the 3.2 mJ input pulse energy, we measured a relative energy content of 78 % for compression from 730 fs down to 56 fs FWHM. This gives an estimated peak power boost of around 8, with a resulting peak power of about 30 GW after post-compression assuming a total transmission of 80%. Another way to quantify the post-compression quality is to look into figures of merit such as the KTQ product introduced in [21], which considers the total transmission T of the compression setup, the compression ratio K achieved, as well as the compressed pulse quality Q, i.e. the relative energy content. The KTQ product is directly proportional to the peak power boost. In the present case, the transmission of the cell itself was about 87% and the transmission of the compressor was 56%, limited by the employed polarization optics and gratings. This results in T=49%, which can be drastically improved by employing a chirped mirror compressor or a double pass grating compressor enabling a compressor transmission above 78% [Grebing_2020]. While our measurements were carried out at a compression ratio of about 13, larger ratios close to 40 have been reported [16], indicating the potential for much larger peak power boosts.

We now extend our study to the entire laser burst containing about 100 pulses.

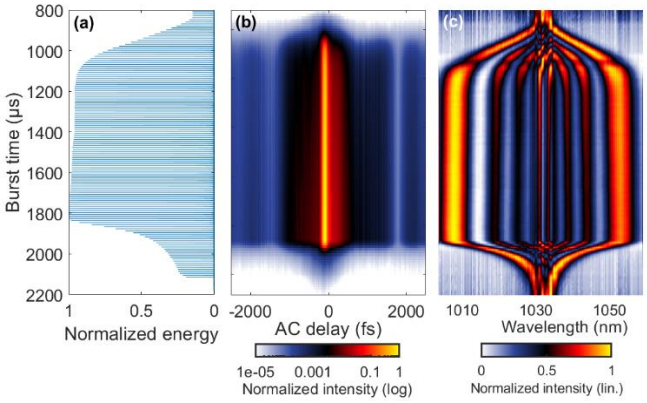

Fig. 3. (a) MPC output pulse energy, showing the burst structure. (b) Full temporal intensity with 10 fs time steps and (c) Intra-burst spectra over the full burst of the post-compressed laser.

Using our home-built automated 3rd order AC, we are able to record high dynamic range AC traces resolving all pulses over the full burst, as shown in Figure 3(b). The 3rd order AC trace resembling the full burst is obtained by combining the recorded UV diode traces of all pulses (separated considering the 100 kHz intra-burst temporal pulse pattern) at different attenuation filter settings. The full AC trace shows that the pulses are well-behaved over the entire flat part of the burst. They also reveal fast dynamics at the leading (Fig.4 (a)) and trailing (b) edges of the burst. Figure 4(c) shows the relative energy content of the main compressed pulse over the flat part of the burst using again an integration window of 2τ. An energy content of 78% is consistently obtained for a duration of 650 μs, i.e. 65 pulses inside the burst, with a standard deviation below 0.2%.

Another parameter which is of particular interest for the MPC output pulses is the broadened spectrum. In order to measure the spectrum of individual pulses inside the burst, a MHz rate spectrograph was employed, based on the linear array detector KALYPSO [22]. Fig.3 (c) presents the resulting spectral mapping for each single pulse within the burst, matching the intra-burst dynamics highlighted in Fig.4 (a) and (b).

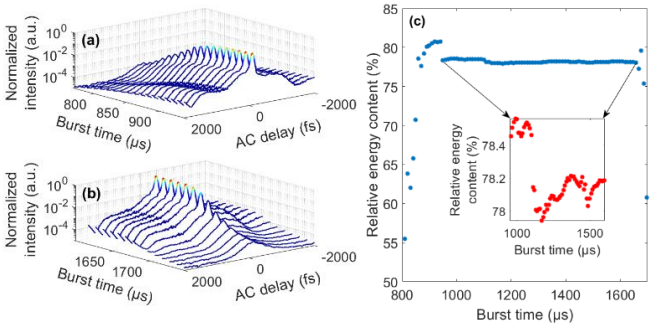

Fig.4. Intra-burst dynamics revealing pulse intensity and temporal contrast variations for leading (a) and trailing (b) edge of the burst. (c) Measured relative energy content over the full burst, with a zoom (inset) on the flat part of the burst showing the very small variations.

Employing our 3rd order AC and the MHz rate spectrograph allows us to perform intra-burst FROG measurements in order to retrieve the phase of the individual post-compressed pulses. The approach is the same as used for the full burst contrast measurement with the UV photodiode being replaced be the fast spectrograph. The pulses are retrieved from the third-harmonic FROG traces using a time-

domain version of the extended ptychographic iterative engine (ePIE) algorithm, which is commonly used for coherent diffractive imaging [23]. Here, the pulse and its second harmonic are treated as object and probe signals. The two signals are iteratively corrected in the frequency domain using the recorded trace. In the time domain, update functions constructed employing the known mathematical form of the trace are used. Both signals are retrieved separately, coupled by their corresponding update functions. An example of a FROG trace obtained for an individual pulse in the burst is shown in Fig. 5(a). In (b), measured and retrieved pulses are shown. Finally, an example of retrieved spectral amplitude and phase is plotted in (c) together with a measured single pulse spectrum recorded with the MHz repetition rate spectrograph.

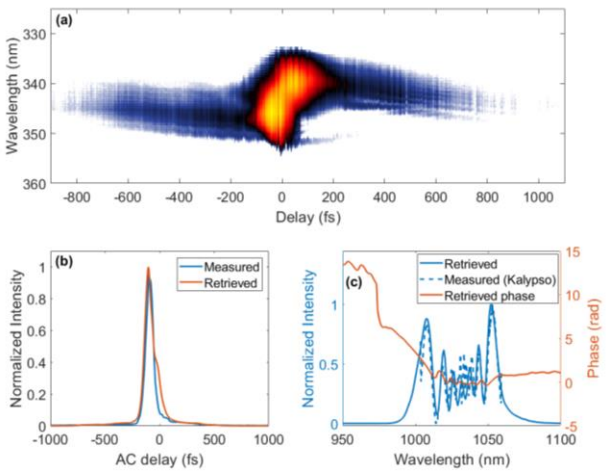

Fig. 5. (a) Example of the FROG trace for the 80th pulse in the burst. The complete burst-resolved FROG traces are shown in the supplementary material (video 1). (b) Measured 3rd order AC trace and retrieved pulse for a single pulse in the burst. (c) corresponding spectrum, recorded by the MHz spectrograph and corrected for standard silicon response in this wavelength range. The supplementary material shows the retrievals for all pulses in the burst (video 2).

In this work we have demonstrated reliable intra-burst pulse characterization at 100 kHz repetition rate allowing us to fully resolve spectrum, phase and temporal contrast of a post-compressed pulse from a high power Yb:YAG burst-mode laser. The combination of a high average power Innoslab amplifier with a gas-filled MPC yield 56 fs pulses at 3.2 mJ with a relative energy content of up to 78% in the main pulse. We showed that a high temporal pulse energy contrast is achieved across the entire flat part of the burst. Our results demonstrate suitability of the employed post-compression-based laser concept for FEL pump-probe experiments and show promising characteristics for the use of such laser systems as efficient drivers for secondary frequency conversion stages. Moreover, the MHz-rate diagnostic tools will be very beneficial for FEL user experiments which require a high degree of control over the burst dynamics.

Funding. Swedish Research Council (2019-06275).

Acknowledgments. We acknowledge DESY (Hamburg, Germany), a member of the Helmholtz Association HGF, for the provision of experimental facilities. Parts of this research were carried out with FLASH2 pump–probe laser and we would like to thank members of the FS-LA group for assistance.

Disclosures. The authors declare no conflicts of interest.

Data availability. Data underlying the results presented in this paper are not publicly available at this time but may be obtained from the authors upon reasonable request.

Supplemental document. See Supplement 1 for supporting content.

References

1. F. Calegari, G. Sansone, S. Stagira, C. Vozzi, and M. Nisoli, J. Phys. B **49**, 062001 (2016).
2. M. Müller, A. Klenke, A. Steinkopff, H. Stark, A. Tünnermann, and J. Limpert, Opt. Lett. **43**, 6037-6040 (2018).
3. B. E. Schmidt, A. Hage, T. Mans, F. Légaré, and H. J. Wörner, Opt. Express **25**, 17549-17555 (2017).
4. T. Nagy, P. Simon, and L. Veisz, Advances in Physics: X, **6**:1, 1845795 (2021).
5. N. G. Khodakovskiy, M. P. Kalashnikov, V. Pajer, A. Blumenstein, P. Simon, M. M. Toktamis, M. Lozano, B. Mercier, Z. Cheng, T. Nagy, and R. Lopez-Martens, Laser Phys. Lett. **16**, 095001 (2019).
6. N. Smijesh, X. Zhang, P. Fischer, A. A. Muschet, R. Salh, A. Tajalli, U. Morgner, and L. Veisz, Opt. Lett. **44**, 4028-4031 (2019)
7. A. Jullien, O. Albert, F. Burgy, G. Hamoniaux, J.-P. Rousseau, J.-P. Chambaret, F. Augé-Rochereau, G. Chériaux, J. Etchepare, N. Minkovski, and S. M. Saltiel, Opt. Lett. **30**, 920-922 (2005).
8. S. Gröbmeyer, K. Fritsch, B. Schneider, M. Poetzlberger, V. Pervak, J. Brons, and O. Pronin, Appl. Phys. B **126**, 159 (2020).
9. F. Köttig, D. Schade, J. R. Koehler, P. St. J. Russell, and F. Tani, Opt. Express **28**, 9099-9110 (2019).
10. C. Grebing, M. Müller, J. Buldt, H. Stark, and J. Limpert, Opt. Lett. **45**, 6250-6253 (2020).
11. B. Faatz, E. Plönjes, et al., New J. Phys. **18**, 06002 (2016).
12. T. Lang, S. Alisauskas, U. Große-Wortmann, T. Hülsenbusch, B. Manschwetus, C. Mohr, J. Müller, F. Peters, N. Schirmel, S. Schulz, A. Swiderski, J. Zheng, and I. Hartl, in 2019 Conference on Lasers and Electro-Optics Europe and European Quantum Electronics Conference, OSA Technical Digest (Optical Society of America, 2019), paper ca_2_1.
13. M. Beye (ed.), *FLASH2020+: Making FLASH Brighter, Faster and More Flexible: Conceptual Design Report*, DESY, Hamburg, Germany (2020).
14. M. Seidel, F. Pressacco, O. Akcaalan, T. Binhammer, J. Darvill, N. Ekanayake, M. Frede, U. Grosse-Wortmann, M. Heber, C. M. Heyl, D. Kutnyakhov, C. Li, C. Mohr, J. Müller, O. Puncken, H. Redlin, N. Schirmel, S. Schulz, A. Swiderski, H. Tavakol, H. Tünnermann, C. Vidoli, L. Wenthaus, N. Wind, L. Winkelmann, B. Manschwetus, and I. Hartl, arXiv:2105.05882v2 (2021).
15. A.-L. Viotti, S. Alisauskas, A. Bin Wahid, P. Balla, N. Schirmel, B. Manschwetus, I. Hartl, and C. M. Heyl, J. Synchrotron Rad. **28**, 36-43 (2021).
16. P. Balla, A. Bin Wahid, I. Sytcevich, C. Guo, A.-L. Viotti, L. Silletti, A. Cartella, S. Alisauskas, H. Tavakol, U. Grosse-Wortmann, A. Schönberg, M. Seidel, A. Trabattoni, B. Manschwetus, T. Lang, F. Calegari, A. Couairon, A. L'Huillier, C. L. Arnold, I. Hartl, and C. M. Heyl, Opt. Lett. **45**, 2572 (2020).
17. J. Schulte, T. Sartorius, J. Weitenberg, A. Vernaleken, and P. Russbueldt, Opt. Lett. **41**, 4511-4514 (2016).
18. P. Russbueldt, T. Mans, G. Rotarius, J. Weitenberg, H. D. Hoffmann, and R. Poprawe, Opt. Express **17**, 12230-12245 (2009).
19. M. Hanna, N. Daher, F. Guichard, X. Délen, and P. Georges, J. Opt. Soc. Am. B **37**, 2982-2988 (2020).
20. E. Escoto et al., manuscript in preparation (2021).
21. P. Russbueldt, J. Weitenberg, J. Schulte, R. Meyer, C. Meinhardt, H. D. Hoffmann, and R. Poprawe, Opt. Lett. **44**, 5222-5225 (2019).
22. C. Gerth, G. Brenner, M. Caselle, S. Düsterer, D. Haack, D. Makowski, A. Mielczarek, S. Palutke, L. Rota, V. Rybnikov, C. Schmidt, B. Steffen, and K. Tiedtke, J. Synchrotron Rad. **26**, 1514-1522 (2019).
23. P. Sidorenko, O. Lahav, Z. Avnat, and O. Cohen, Optica **3**, 1320 (2016).

Full reference list

1. F. Calegari, G. Sansone, S. Stagira, C. Vozzi, and M. Nisoli, "Advances in attosecond science," J. Phys. B **49**, 062001 (2016).
2. M. Müller, A. Klenke, A. Steinkopff, H. Stark, A. Tünnermann, and J. Limpert, "3.5 kW coherently combined ultrafast fiber laser," Opt. Lett. **43**, 6037-6040 (2018).
3. B. E. Schmidt, A. Hage, T. Mans, F. Légaré, and H. J. Wörner, "Highly stable, 54 mJ Yb-Innoslab laser platform at 0.5 kW average power," Opt. Express **25**, 17549-17555 (2017).
4. . Nagy, P. Simon, and L. Veisz, "High-energy few-cycle pulses: post-compression techniques," Advances in Physics: X, **6**:1, 1845795 (2021).
5. N. G. Khodakovskiy, M. P. Kalashnikov, V. Pajer, A. Blumenstein, P. Simon, M. M. Toktamis, M. Lozano, B. Mercier, Z. Cheng, T. Nagy, and R. Lopez-Martens, "Generation of few-cycle laser pulses with high temporal contrast via nonlinear elliptical polarization rotation in a hollow fibre compressor," Laser Phys. Lett. **16**, 095001 (2019).
6. N. Smijesh, X. Zhang, P. Fischer, A. A. Muschet, R. Salh, A. Tajalli, U. Morgner, and L. Veisz, "Contrast improvement of sub-4 fs laser pulses using nonlinear elliptical polarization rotation," Opt. Lett. **44**, 4028-4031 (2019)
7. A. Jullien, O. Albert, F. Burgy, G. Hamoniaux, J.-P. Rousseau, J.-P. Chambaret, F. Augé-Rochereau, G. Chériaux, J. Etchepare, N. Minkovski, and S. M. Saltiel, "10^{-10} temporal contrast for femtosecond ultraintense lasers by cross-polarized wave generation," Opt. Lett. **30**, 920-922 (2005).
8. S. Gröbmeyer, K. Fritsch, B. Schneider, M. Poetzlberger, V. Pervak, J. Brons, and O. Pronin, "Self-compression at 1 µm wavelength in all-bulk multi-pass geometry," Appl. Phys. B **126**, 159 (2020).
9. F. Köttig, D. Schade, J. R. Koehler, P. St. J. Russell, and F. Tani, "Efficient single-cycle pulse compression of an ytterbium fiber laser at 10 MHz repetition rate," Opt. Express **28**, 9099-9110 (2019).
10. C. Grebing, M. Müller, J. Buldt, H. Stark, and J. Limpert, "Kilowatt-average-power compression of millijoule pulses in a gas-filled multi-pass cell," Opt. Lett. **45**, 6250-6253 (2020).
11. B. Faatz, E. Plönjes, et al., "Simultaneous operation of two soft x-ray free-electron lasers driven by one linear accelerator," New J. Phys. **18**, 06002 (2016).
12. T. Lang, S. Alisauskas, U. Große-Wortmann, T. Hülsenbusch, B. Manschwetus, C. Mohr, J. Müller, F. Peters, N. Schirmel, S. Schulz, A. Swiderski, J. Zheng, and I. Hartl, "Versatile OPCPA Pump-Probe Laser System for the FLASH2 XUV FEL beamline at DESY," in 2019 Conference on Lasers and Electro-Optics Europe and European Quantum Electronics Conference, OSA Technical Digest (Optical Society of America, 2019), paper ca_2_1.
13. M. Beye (ed.), *FLASH2020+: Making FLASH Brighter, Faster and More Flexible: Conceptual Design Report*, DESY, Hamburg, Germany (2020).
14. M. Seidel, F. Pressacco, O. Akcaalan, T. Binhammer, J. Darvill, N. Ekanayake, M. Frede, U. Grosse-Wortmann, M. Heber, C. M. Heyl, D. Kutnyakhov, C. Li, C. Mohr, J. Müller, O. Puncken, H. Redlin, N. Schirmel, S. Schulz, A. Swiderski, H. Tavakol, H. Tünnermann, C. Vidoli, L. Wenthaus, N. Wind, L. Winkelmann, B. Manschwetus, and I. Hartl, "Ultrafast MHz-rate burst-mode pump-probe laser for the FLASh FEL facility based on nonlinear compression of ps-level pulses from an Yb-amplifier chain," arXiv:2105.05882v2 (2021).
15. A.-L. Viotti, S. Alisauskas, A. Bin Wahid, P. Balla, N. Schirmel, B. Manschwetus, I. Hartl, and C. M. Heyl, "60 fs, 1030 nm FEL pump-probe laser based on a multi-pass post-compressed Yb:YAG source," J. Synchrotron Rad. **28**, 36-43 (2021).
16. P. Balla, A. Bin Wahid, I. Sytcevich, C. Guo, A.-L. Viotti, L. Silletti, A. Cartella, S. Alisauskas, H. Tavakol, U. Grosse-Wortmann, A. Schönberg, M. Seidel, A. Trabattoni, B. Manschwetus, T. Lang, F. Calegari, A. Couairon, A. L'Huillier, C. L. Arnold, I. Hartl, and C. M. Heyl, "Postcompression of picosecond pulses into the few-cycle regime," Opt. Lett. **45**, 2572 (2020).
17. J. Schulte, T. Sartorius, J. Weitenberg, A. Vernaleken, and P. Russbueldt, "Nonlinear pulse compression in a multi-pass cell," Opt. Lett. **41**, 4511-4514 (2016).
18. P. Russbueldt, T. Mans, G. Rotarius, J. Weitenberg, H. D. Hoffmann, and R. Poprawe, "400 W Yb:YAG Innoslab fs-amplifier," Opt. Express **17**, 12230-12245 (2009).
19. M. Hanna, N. Daher, F. Guichard, X. Délen, and P. Georges, "Hybrid pulse propagation model and quasi-phase-matched four-wave mixing in multipass cells," J. Opt. Soc. Am. B **37**, 2982-2988 (2020).
20. E. Escoto et al., manuscript in preparation (2021).
21. P. Russbueldt, J. Weitenberg, J. Schulte, R. Meyer, C. Meinhardt, H. D. Hoffmann, and R. Poprawe, "Scalable 30 fs laser source with 530 W average power," Opt. Lett. **44**, 5222-5225 (2019).
22. C. Gerth, G. Brenner, M. Caselle, S. Düsterer, D. Haack, D. Makowski, A. Mielczarek, S. Palutke, L. Rota, V. Rybnikov, C. Schmidt, B. Steffen, and K. Tiedtke, "Linear array detector for online diagnostics of spectral distributions at MHz repetition rates," J. Synchrotron Rad. **26**, 1514-1522 (2019).
23. P. Sidorenko, O. Lahav, Z. Avnat, and O. Cohen, "Ptychographic reconstruction algorithm for frequency-resolved optical gating: super-resolution and supreme robustness,"Optica **3**, 1320-1330 (2016).